Catalysis Letters
https://doi.org/10.1007/s10562-018-2441-1

On the Surface Nature of Bimetallic PdZn Particles Supported on a ZnO–CeO_2 Nanocomposite for the Methanol Steam Reforming Reaction

Celina E. Barrios[1] · Miguel A. Baltanás[1] · Marta V. Bosco[1] · Adrian L. Bonivardi[1,2]

Received: 16 February 2018 / Accepted: 30 May 2018

Abstract

CO adsorption—as a molecular probe—was studied by transmission IR spectroscopy on pre-reduced Pd and bimetallic PdZn nanoparticles. Palladium was supported (2 wt% Pd) on pure CeO_2, ZnO and a ZnO–CeO_2 composite (atomic ratio Zn:Ce = 1:2). The Pd $3d_{5/2}$ binding energy shift, together with the formation of metallic zinc were consistent with the development of a PdZn alloy over the zinc-containing supports at increasing reduction temperature, as revealed by XPS. Following H_2 reduction at 623 K the bimetallic particles showed only linear CO adsorption (CO_L) at initial contact time (10 Torr CO, 298 K), giving rise to a convoluted IR band ascribed to different Pd sites, where it was assumed that the Pd–Pd distances were larger than for pure Pd crystallites, indicating the presence of a PdZn alloyed surface. However, for longer exposure time to CO and/or higher superimposed pressure, the appearance of bridge and hollow coordinated CO (CO_B and CO_H, respectively) on the Pd sites suggested the degradation of the PdZn surface alloy, most likely due to the segregation of Pd surface patches. The temperature-programmed, dynamic isobaric adsorption of CO (TPA-CO), under flowing CO(1%)/He on the catalysts pre-reduced at 623 K (that is, for similar conditions to those found in the methanol steam reforming—MSR-process) showed faster desorption of CO_L as compared to $CO_B + CO_H$ species for supported Pd/CeO_2, as expected. However, the TPA-CO results on Pd/ZnO–CeO_2 were atypical: even under the superimposed, low CO partial pressure, and for a temperature range similar to those found at high methanol conversion in the MSR reaction, the PdZn bimetallic surface nature was recovered, which could be an explanation of the good selectivity to CO_2 of Pd/ZnO-based catalysts and—in particular—of the catalytically stable Pd/ZnO–CeO_2 materials.

Graphical Abstract

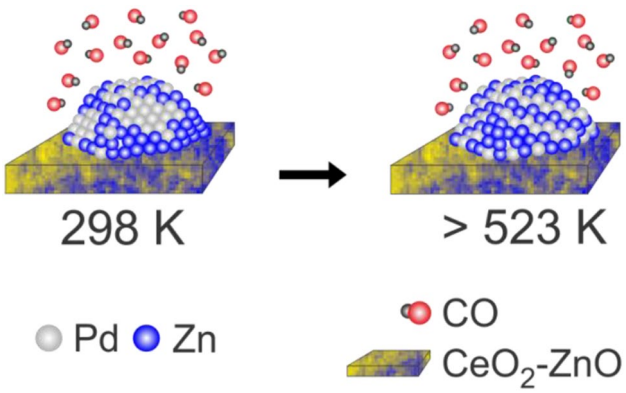

Electronic supplementary material The online version of this article (https://doi.org/10.1007/s10562-018-2441-1) contains supplementary material, which is available to authorized users.

Extended author information available on the last page of the article

Published online: 20 June 2018

Keywords H_2 production · Alcohol reforming · Ceria · Fuel cells

1 Introduction

Diverse strategies are currently applied for the study of single crystal palladium alloys as well as bimetallic palladium-supported catalysts (e.g., Au–Pd [1], Ag–Pd [2], Pt–Pd [3], Pd–Ga [4–6] and Pd–Zn [6–11]), by employing infrared (IR) spectroscopy together with other characterization techniques such as high resolution electron microscopy (HRTEM), X-ray photoelectron spectroscopy (XPS) and/or extended X-ray absorption spectroscopy (EXAFS).

Carbon monoxide has been extensively used as a probe molecule to test the surface of pure or intermetallic Pd-based catalysts. From the analysis of the type of coordination of adsorbed-CO, IR spectroscopy can bring direct information in regards the geometric surface arrangement of metallic palladium atoms [12]. So, the absence of absorption bands, proper of multiply coordinated chemisorbed CO in PdZn and Pd_2Ga alloys, has been found to be sensitive for the detection of Pd–Pd distances larger than that of pure, metallic Pd [12–14].

The knowledge of the surface composition and structure of these bimetallic palladium catalysts under technological reaction conditions, in particular for methanol steam reforming (MSR), has proved to be a difficult task, because pressure, temperature and gas composition (reactants/products) can strongly modify these features and even build (or destroy) catalytic active sites. The model catalyst approach has been recently applied to PdZn near-surface alloys generated on Pd(111) and/or Pd foil (see, for example [15]), to study their thermal stability under ultra-high vacuum [13] and close-to-real conditions [15]. Contemporarily, Föttinger et al. studied the dynamic structure of a working MSR catalyst, Pd/ZnO nanoparticles, proving for the first time that a PdZn bulk alloy formed in the course of the catalytic reaction is responsible for the remarkable selectivity to CO_2 and H_2 from the methanol/water reaction mixture [11].

It is also interesting to point out the effort put into the study of the activation of H_2O by these model systems [15]. Yet, selective and stable novel catalysts based on PdZn bimetallic nanoparticles supported on a reactive oxide such as ceria (prepared by impregnating ZnO–CeO_2 nanocomposites [16]) have a greater degree of complexity. In this last case, H_2O activation could no longer be an issue, nor the rate-determining-step for MSR, since said activation has been ascribed to CeO_2 in both MSR [16] and the water gas shift (WGS) reaction [16, 17]. Moreover, under high conversion conditions in the MSR process, the catalysts are exposed to an atmosphere rich in CO_2 and H_2 but CO is also present, as a byproduct of the reverse WGS reaction. Carbon monoxide has a strong adsorption energy on palladium and could be the responsible of PdZn decomposition and/or, in other words, of the decrease in CO_2 selectivity [18, 19]. Since it is well documented that CO alone has already a strong influence on the dynamic reconstruction of metal surfaces, the presence of carbon monoxide is expected to induce surface modifications, which can be particularly relevant under realistic reaction conditions [20].

The degradation of the intermetallic PdZn surface can be more o less relevant depending on the temperature and pressure of the adsorbate/s [16]. It seems then reasonable to investigate further the nature and stability of the alloyed PdZn surface on supported bimetallic nanoparticles under the presence of CO.

On these grounds, the aim of this work was to study the static and dynamic adsorption of CO on ceria-supported bimetallic PdZn catalysts, which were pre-reduced in H_2 at different temperatures, under a constant superimposed CO pressure (7.6 Torr) similar to the one found in our previous studies of the steam reforming of methanol for a broad range of alcohol conversion [16]. In addition, the pre-reduced catalysts were exposed to CO_2 prior to carbon monoxide chemisorption.

2 Experimental

2.1 Catalysts

The supported Pd catalysts were prepared by incipient wetness impregnation of acetone-diluted $Pd(AcO)_2$ (Sigma 99.97% Pd) onto pure zinc and cerium oxides, as well as on a *composite* of both oxides, at room temperature (RT).

The pure oxides and the composite (from now on designated ZnO–CeO_2, containing a atomic ratio Zn:Ce = 1:2) were synthesized by precipitating (or co-precipitating) the metal nitrates with ammonium carbonate. The supports' precursors were dried in vacuo (393 K, 4 h) and calcined in a glass reactor using synthetic air, heating from 298 to 673 K at 3 K/min and then holding 673 K for 2 h.

2 wt% Pd was added to the pure ZnO, CeO_2, and the ZnO–CeO_2 composite. After vacuum drying (333 K, 2 h), the impregnated supports were decomposed in the glass reactor using synthetic air, heating from 298 to 673 K at 3 K/min and then holding 673 K for 2 h. The materials were then crushed and sieved. Only the +40/−80 Tyler mesh fractions were kept, stored in a desiccator prior to use. Table 1 contains appropriate structural information about these catalysts. Noteworthily, this preparation method gave macro–mesoporous supports with moderate S_{BET} and reasonable pore-related (i.e., V_p and d_p) valued, which made

Table 1 Morphological and structural properties of the supported Pd catalysts

Catalyst	Abridged designation	S_{BET} [a] (m^2/g)	V_p [b] (cm^3/g)	d_p [c] (nm)	Support crystal size[d] (nm)		Pd SEF[e] (%)	
					ZnO	CeO_2	H_2 prereduction temperature	
							423 K	623 K
(2 wt%) Pd/CeO_2	Pd/CeO_2	80	0.04	1.3	–	12.4	26	25
(2 wt%) Pd/ZnO–CeO_2	Pd/ZnO–CeO_2	50	0.015	1.3	31.4	10.1	13	8
(2 wt%) Pd/ZnO	Pd/ZnO	8	0.002	1.4	78.9	–	5[f]	1.2

[a]BET (LN_2) specific surface

[b]Pore volume

[c]Barrett–Joyner–Halenda (BJH) pore diameter

[d]By X-ray diffraction after Rietveld refinement [21]

[e]SEF = surface exposed fraction (by step CO chemisorption, at 298 K [16]) after pre-reduction under pure H_2 (1 h) at said T_{redn}

[f]Pre-reduction under pure H_2 at 298 K (24 h)

them suitable for the study of the pursued catalytic reaction, the steam reforming of methanol. Moreover, the nanostructural characterization of the composite, followed by refined XRD analysis, allowed to conclude that Zn(II) cation was not incorporated into the ceria lattice. Instead, the crystalline domains of ZnO were smaller (~ 30 nm) in the nanocomposite than in pure zinc oxide (~ 110 nm), while the ceria crystal size was constant for the pure CeO_2 and the ZnO–CeO_2 *nanocomposite*. Coprecipitation with ceria aided to the "fragmentation" of ZnO domains and, furthermore, an amorphous portion of ZnO—higher than 20%—was anticipated on the *nanocomposite* [16].

The surface exposed metal fraction (SEF) of palladium was determined by step CO chemisorption at RT, using a dilute CO (1%)/He stream and a conventional, calibrated TCD signal. The catalysts were pre-reduced under H_2 flow from RT to the designated reduction temperature (5 K/min), holding for 1 h. Pure He was then passed (623 K, 30 min), cooling under flow down to RT prior to introducing the CO step. The amount of adsorbed CO was computed by measuring the elapsed time between the initial switching to the CO/He stream and the breakthrough time signal (< 8 min of contact time, which assures an overestimation of the SEF lower than 10% for a CO:Pd_s = 1:1 stoichiometry, where Pd_s stands for a surface palladium atom). Detailed characterization data of the complete set of supported Pd catalysts (prepared by employing different Zn:Ce atomic ratios), as well as their performance in the MSR reaction for a broad range of process conditions, is given elsewhere [16, 21].

2.2 X-Ray Photoelectron Spectroscopy (XPS)

XPS measurements were carried out using a multi-technique SPECS unit furnished with a hemispherical PHOIBOS 150 analyzer, operating in the fixed analyzer transmission (FAT) mode. The spectra were obtained using the Al *K*α X-ray source (@ 200 W and 12 kV; pass energy = 30 eV). Each sample was treated in situ in a pretreatment chamber attached to the main XPS chamber as follows: (i) at 623 K in O_2 (5%)/Ar flow for 10 min and (ii) at 423 and 623 K in H_2 (5%)/Ar flow, for 10 min each time (heating ramp for each pretreatment = 10 K/min). After each treatment, the samples were transferred to the analysis chamber without exposure to air (base pressure = 2×10^{-8} Pa). Ce 3d, C 1s, O 1s, Pd 3d, Zn 2p core levels and Zn LMM Auger signals were recorded (the C 1s signal at 285 eV was used as reference).

Shirley-type background and a 70:30 ratio of Gaussian-to-Lorentzian functions were used for data treatment, employing the Casa XPS program (Casa Software Ltd, UK). For the quantification of the elements, sensitivity factors provided by the manufacturer were used.

2.3 Infrared Carbon Monoxide Adsorption Studies

The supported metal (either Pd or PdZn bimetallic) particles were studied by Fourier-transformed infrared spectroscopy (FTIR) in the transmission mode, using carbon monoxide as a molecular probe. A Nicolet Magna 550 series II spectrometer, featuring a MCT-A detector, was employed. Self-supported wafers (13 mm diameter, ~ 30 mg/ea., pressed at 4 ton/cm^2) were placed, in turn, into a Pyrex® IR cell, with water-cooled NaCl windows, which was attached to a conventional high-vacuum system (base pressure = 1.33×10^{-4} Pa) equipped with a manifold for gas flow and dosage. Infrared spectra were acquired every 2 min, averaging 100 scans (4 cm^{-1} resolution) and normalized by pellet weight.

The selected range of CO adsorption pressures was similar to the one the catalysts were exposed to during their MSR performance studies [16]. Ultra high purity He, N_2 and

H_2 (99.999%) supplied by INDURA (Air Liquide Argentina), together with research grade CO (99.99%) and CO_2 (99.996%), supplied by AGA (Linde Argentina) were used. A calibrated CO (1%)/He mixture (He purity: 99.999%) was also employed. Oxygen and water impurities were removed with MnO/Al_2O_3 and 3 Å molecular sieve (Fisher Co.) traps, respectively.

The infrared spectra were processed using the Origin® software package, solving specific signals with Lorentzian and/or Gaussian functions to determine integrated absorbance and/or peak intensity, where appropriate. The background absorption corresponding to the pre-reduced and evacuated sample, at room temperature, was subtracted from each spectrum.

2.3.1 Static Adsorption of CO

Prior to the adsorption measurements, the catalysts were pre-reduced in situ in pure H_2 (50 cm^3/min), heating from 298 K to the desired final reduction temperature (T_{redn}) between 423 and 623 K, in each case at 3 K/min and holding at said temperature for 1 h. Then, the catalysts were evacuated at 623 K (30 min) and cooled to RT in vacuo.

Two experimental protocols were used for studying the static adsorption of CO at RT. In the first one (protocol A), CO was chemisorbed twice onto the pre-reduced, evacuated catalysts, as per the following sequence: (i) CO adsorption at 10 and 50 Torr (10 min/ea., 298 K); (ii) evacuation (5 min, 298 K); (iii) heating, in vacuo, to 623 K (temperature-programmed desorption—TPD-, 5 K/min, holding 30 min); (iv) cooling, in vacuo, to 298 K; and (v) re-adsorption of CO as in step (i). Different, fresh samples were used for each H_2 pre-reduction temperature. In the second protocol (protocol B), the pre-reduced (623 K), evacuated catalysts were exposed to CO_2 prior to studying CO chemisorption, as per the following sequence: (i) CO_2 adsorption at 10, 50, 70 and 100 Torr (10 min/ea., 298 K); (ii) evacuation (30 min, 298 K); and (iii) CO adsorption at 10 and 50 Torr (10 min/ea., 298 K).

2.3.2 Dynamic (Isobaric) Adsorption of CO

A single protocol, using isobaric temperature-programmed adsorption of CO (TPA-CO), was employed. The catalysts were previously reduced in situ under flowing H_2 (50 cm^3/min), heating from 298 to 623 K (3 K/min), and holding at the maximum temperature for 1 h. Then, the catalysts were evacuated at 623 K (30 min) and cooled in vacuo down to RT, after which they were exposed to a 50 cm^3/min stream of dilute CO (1%)/He (i.e., ~7.6 Torr CO) at 298 K for 30 min, and then heated under the flowing mixture (5 K/min) up to 623 K, at 1 bar. Because of the low surface area of the zinc oxide, and the consequent low dispersion of the metal particles at the 2 wt% loading (Table 1) the Pd/ZnO catalyst could not be studied by this TPA-CO technique.

3 Results and Discussion

3.1 Bimetallic PdZn Particles

Particularly, we report here some quantitative XPS results for these supported Pd catalysts (Table 2). Both, the Pd 3d and Zn LMM signals can be interpreted in the light of the formation of a PdZn alloy phase. The Pd 3d signal on Pd/CeO_2 shifted from 337.0 to 335.3 eV after the reduction with H_2 at each temperature used (that is, 473 and 623 K), which is characteristic of the Pd^{2+} reduction to metallic palladium (Pd^0 state) [22]. However, for $Pd/ZnO–CeO_2$ and Pd/ZnO, the Pd 3d signals ($3d_{3/2}$ and $3d_{5/2}$) could not be appropriately fitted with just one band component after H_2 reduction. On these two reduced catalysts a shifting of the electron binding energy of approximately − 1.8 and − 1.0 eV (for 423 and 623 K, respectively) was observed with respect to the location of the Pd $3d_{5/2}$ band on the oxidized materials, together with an increase of the full width at half maximum (FWHM). This is in agreement with the presence of multiple chemical states of reduced Pd, which can be interpreted as the convolution of two signals proper of pure Pd^0 and Zn-alloyed Pd^0 (that is, Pd^0 in PdZn), as shown in Fig. 1. Based on the previous assumption the percentage of alloyed Pd was estimated and so it can be anticipated that after H_2 pre-reduction at 623 K during 60 min more than 90% of palladium is alloyed to Zn in both the $Pd/ZnO–CeO_2$ and Pd/ZnO catalysts (see Table 2, column 7). These results are congruent with previous temperature-programmed H_2-reduction studies of PdO supported on bulk Zn which have shown that it is possible to form a Pd–Zn alloy above 548 K [7–11, 15, 23, 24].

Hence, zinc oxide should (at least partially) be reduced. The small shifting of electron binding energy for Zn $2p_{3/2}$ between metallic Zn and ZnO is a constraint to prove ZnO reduction. Therefore, we studied the most intense Zn $L_2M_{45}M_{45}$ and $L_3M_{45}M_{45}$ Auger signals, which are highly sensitive for detecting the chemical shift between both oxidation states of zinc, Zn^{2+} and Zn^0 (more than 3–4 eV) [25]. These Auger processes are characterized by five final states (that is, ^1S, ^1G, ^3P, ^1D, and ^3F). Two of these final states can explain approximately 90% of each process (~65 and ~25% for ^1G and ^3F, respectively), while the ^3P and ^1D states (~9%) are strongly convoluted with the ^1G signal [26]. Then, it seems reasonable to solve the $L_3M_{45}M_{45}$ signal (which is roughly twice more intense than the L_2 one) using three overlapped bands corresponding to ^1S, ^1G (which includes the overlapped ^3P and ^1D contributions) and ^3F final states [26].

Table 2 Pd and Zn XPS results for the supported Pd catalysts

Catalyst	Pretreatment[a]	BE Pd $3d_{5/2}$ (eV)			Pd_T [b] (%)	Pd^0_{PdZn} [c] (%)	KE Zn $L_3M_{45}M_{45}$ [d] (eV)		Zn_T [e] (%)	Zn^0 [f] (%)	Pd $_{PdZn}$/Zn[g] (atom/atom)
		Pd^{2+}	Pd^0	Pd^0 (in PdZn)			Zn^{2+}	Zn^0			
Pd/CeO_2	O_2, 623 K	337.0	–	–	13.8	–	–	–	–	–	–
	H_2, 423 K	–	335.3	–	13.4	–	–	–	–	–	–
	H_2, 623 K	–	335.3	–	12.8	–	–	–	–	–	–
Pd/ZnO–CeO_2	O_2, 623 K	336.9	–	–	9.4	–	988.5	–	50.0	–	–
	H_2, 423 K	–	335.1	335.8	9.7	37	988.4	992.4	47.0	12	0.66
	H_2, 623 K	–	335.2	335.9	8.5	86	988.5	992.5	52.1	23	0.64
	H_2, 623 K[h]	–	335.3	335.9	8.7	92	988.6	992.6	50.2	21	0.74
Pd/ZnO	O_2, 623 K	336.6	–	–	2.4	–	988.2	–	97.6	–	
	H_2, 423 K	–	334.7	335.6	3.5	25	988.4	992.4	96.5	12	0.25
	H_2, 623 K	–	334.7	335.6	2.8	92	988.4	992.4	97.2	14	0.19

[a]Oxidation [O_2 (5%)/Ar] or reduction [H_2 (5%)/Ar] at the given temperatures, during 10 min

[b]Atomic percentage of total Pd, based on metallic elements [that is, Pd/(Pd + Zn + Ce); Pd 3d, Zn 2p and Ce 3d signals]

[c]Atomic percentage of Pd^0 forming the PdZn alloy, based on total metallic palladium [that is, $Pd^0/Pd^0 + Pd^0$(in PdZn); Pd $3d_{5/2}$ signal]

[d]Peak position of the ^{1}G final state

[e]Atomic percentage of total Zn, based on metallic elements [that is, Zn/(Pd + Zn + Ce); Pd 3d, Zn 2p and Ce 3d signals]

[f]Atomic percentage of Zn^0, based on total zinc [that is, $Zn^0/(Zn^{2+}+Zn^0)$, Zn $L_3M_{45}M_{45}$]

[g]Atomic ratio between reduced palladium in the PdZn alloy and reduced zinc, calculated from the Pd $3d_{5/2}$ and Zn $2p_{3/2}$ signals. The Zn $2p_{3/2}$ signal intensity was multiplied by the percentage of reduced zinc obtained from the Zn $L_3M_{45}M_{45}$ [Zn^0 (%)]

[h]Reduction [H_2 (5%)/Ar] at said temperature during 60 min

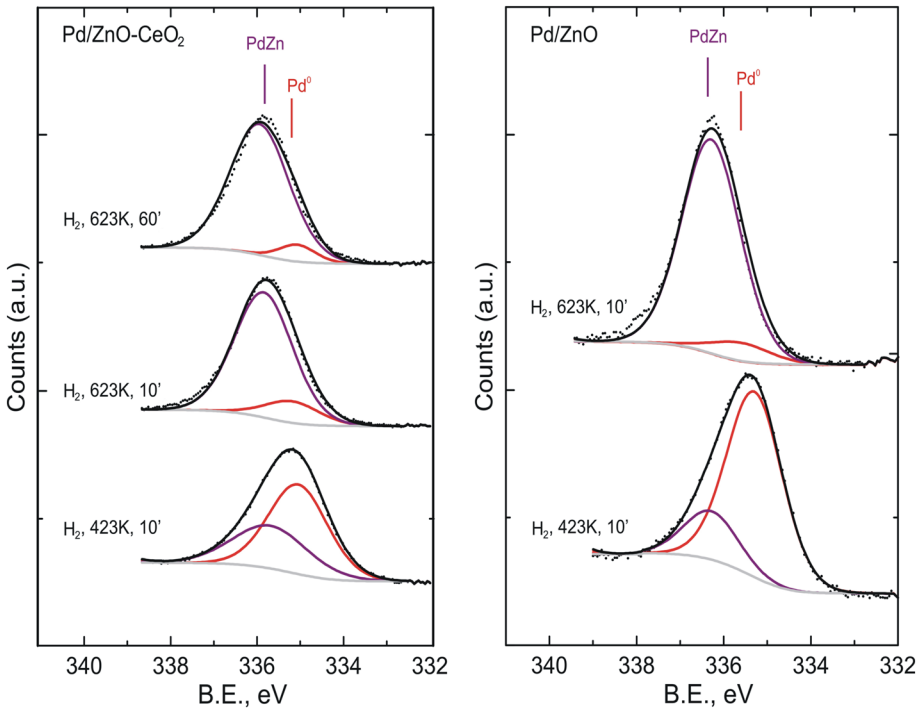

Fig. 1 Deconvoluted XPS spectra of the Pd $3d_{5/2}$ peak for the pre-reduced zinc-containing catalysts. Reducing conditions: H_2 (5%)/Ar at 423 or 623 K, during 10 or 60 min

Figure 2 shows the results of the deconvolution of the Zn $L_3M_{45}M_{45}$ signal, and Table 2 summarizes the KE values for the main peak position (^{1}G final state), and the percentages of total surface zinc and reduced surface zinc (Zn^0). The last one was calculated using the integrated L_3 $M_{45}M_{45}$ areas for the $Zn^0/(Zn^0 + Zn^{2+})$ ratio (see footnote in Table 2).

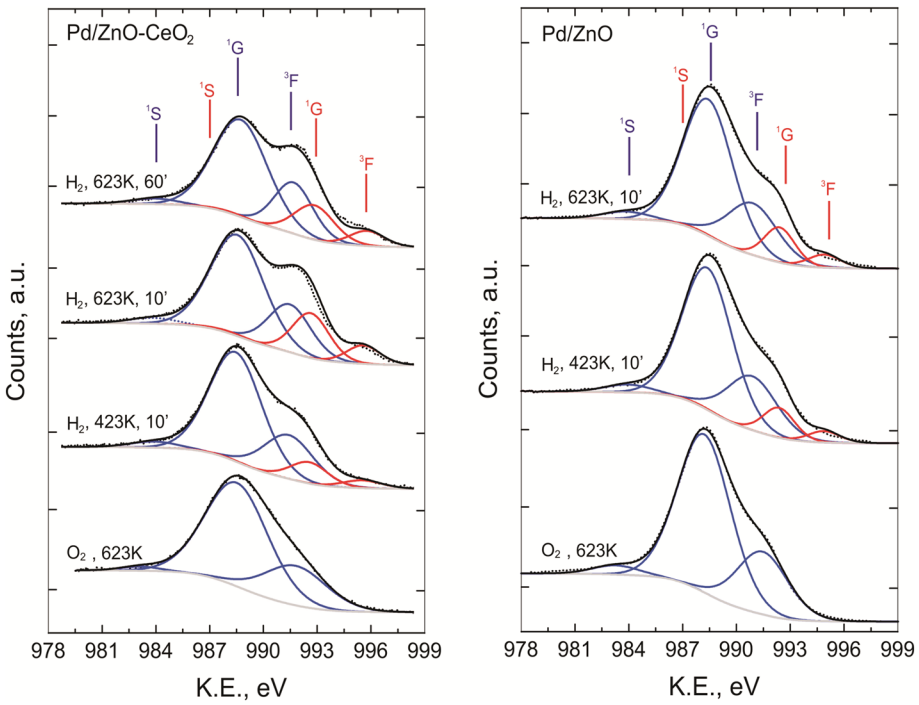

Fig. 2 Auger spectra of the Zn $L_3M_{45}M_{45}$ signal for the Pd/ZnO–CeO_2 and Pd/ZnO catalysts after oxidation in O_2 (5%)/Ar at 623 K (10 min) followed by reduction at increasing temperature, and time of exposure under H_2 (5%)/Ar. Final states (^{1}S, ^{1}G, and ^{3}F) are indicated for the Zn^{2+} (blue) and Zn^0 (red) species

There is an excellent agreement between the main peak position (^{1}G final state) for the Zn^{2+} and Zn^0 species (988.4 and 992.5 eV, respectively) in our oxidized and reduced catalysts and the values reported in the literature for ZnO and Zn (988.2 and 992.5 eV, respectively). At the lowest reduction temperature (T_{redn} = 423 K) Zn^{2+} is already partially reduced to Zn^0; this percentage increased at higher reduction temperature, to maximum values of 21 and 14% for Pd/ZnO–CeO_2 and Pd/ZnO, respectively. Moreover, the atomic ratio between reduced palladium in the PdZn alloy and reduced zinc (last column in Table 2) shows that the amount of Zn^0 was always high enough to obtain the more stable β_1-PdZn phase (see below). The previous observations are consistent with the formation of a PdZn alloy, which was more extensive for the highest reduction temperature employed in our experiments.

These bulk metallic alloy formation results are in complete agreement with our previously reported transmission electron microscopy (TEM) findings, where the high-resolution TEM images of both Pd/ZnO–CeO_2 and Pd/ZnO catalysts, pre-reduced at 623 K (and air passivated), only showed the diffracting crystal planes of PdZn nanoalloy [16].

3.2 Static Adsorption of CO

Several infrared bands, corresponding to the stretching of the C–O bond [ν(CO)] of the carbon monoxide molecule, appear in the IR spectra whenever CO chemisorbs on metal surface sites. On supported palladium, CO may chemisorb in monocoordinated (or on-top, or linear, L), dicoordinated (or bridged, B) and/or tricoordinated (or hollow, H) forms. Typically, the wavenumbers of these different Pd–CO bonds are located in the following order: $\nu(CO_L) > 2000$ cm^{-1}, $1900 < \nu(CO_B) < 2000$ cm^{-1}, and $\nu(CO_H) < 1890$ cm^{-1} [27–31]. In addition, the CO_L and CO_B signals are usually constituted by convoluted pairs of bands, the first pair located approximately at 2080–2060 and 2050–2040 cm^{-1} (from now on signals L_{II} and L_{III}, respectively), and the second one at 1995–1970 and 1950–1900 cm^{-1} (from now on B_I and B_{II}, respectively) [29].

Figure 3 shows the IR spectra in the 2300–1700 cm^{-1} region corresponding to the chemisorption of CO on the catalysts pre-reduced at 623 K (protocol A, step i). On Pd/CeO_2, the typical CO_L and CO_B bands could be readily observed at 0 min (that is, spectra acquired during the first 10 s) upon exposure of the catalyst to 10 Torr CO. At increasing exposure time under this pressure, and moreover at 50 Torr (10 min), the CO_B signal grew considerably, and the CO_H band was then also evident, which is usually ascribed to the restructuring of the palladium particles originated by the strong interaction between the adsorbate and the metal [29].

In terms of the Blyholder's model, the CO chemisorption onto metallic surfaces involves a CO → M σ bond combined with electron retrodonation from the *d* orbitals of the metal atom(s) to the 2π* molecular orbital of the adsorbate, which reduces the force constant of the C–O bond [30]. This simple model, together with abundant spectroscopic information from surface science studies, has allowed the interpretation of the experimental results reported in the literature related

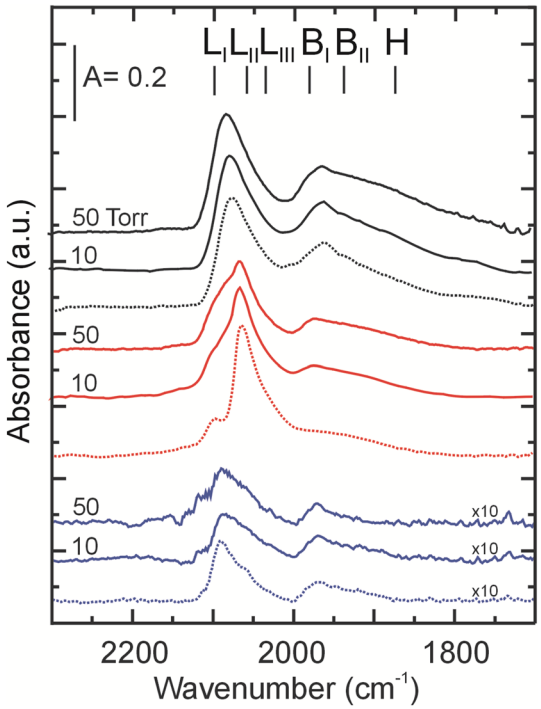

Fig. 3 Static chemisorption of CO at RT on the Pd/CeO_2 (black), Pd/ZnO–CeO_2 (red), and Pd/ZnO (blue) catalysts pre-reduced in pure H_2 at 623 K. Dashed and full lines correspond to 0 and 10 min exposure time, respectively

to the L, B and H infrared bands. Maybe one of the most conducive contributions with regard to alumina-supported Pd, with different degrees of dispersion, is that of Lear et al. [28]. For the particular case of the CO_L convoluted signals on highly disperse Pd, these authors assigned them to CO species linearly adsorbed onto the metal crystallite corners (~ 2080 cm^{-1}) and (111)/(111), and 111/(100) edges (~ 2050 cm^{-1}), respectively. This assignment may plausibly apply to the CO chemisorbed onto the Pd particles supported on ceria as well.

Mostly CO_L species were observed on Pd/ZnO upon the introduction of 10 Torr CO (0 min). With further elapsed time and/or higher CO dosing (50 Torr), though, the CO_B band was also identified, albeit in lower proportion than on Pd/CeO_2. Just linearly bonded CO dominated the initial IR spectra (i.e., 10 Torr CO, 0 min) of the Pd/ZnO–CeO_2 catalyst prepared with the *composite* support.

After Pd–Zn alloy formation, the CO_L signals predominate over the CO_B bands. The latter may even disappear whenever the surface Pd atoms become geometrically apart from each other or when their interatomic distance increases so as to prevent the formation of bridged and hollow-adsorbed CO species [7, 14]. Furthermore, the L_{II} band was the only one that still prevailed at the highest temperature during the TPA-CO experiments (see below).

Along these lines, in a recent work by Rupprechter and coworkers [12] using temperature-programmed CO desorption (TPD-CO) and polarization-modulated infrared reflection absorption spectroscopy (PM-IRAS) at 100 K combined with DFT calculations, evidence was provided for the rearrangement of Pd and Zn atoms on the surface by considering alloys of PdZn/Pd(111) with model "zigzag" structure in the presence of CO. The reconstructed surface was calculated to be more stable in the case of high CO coverage and capable of adsorbing CO on top of Pd atoms up to a saturation coverage of ½ monolayer (ML). The calculated vibrational frequency and adsorption energy of the chemisorbed CO_L onto these arrays were 2067 cm^{-1} and 0.64 eV, respectively, for ½ ML CO coverage and four-layer-thick PdZn surface alloy. They also considered the formation of a PdZn alloy with an array of Pd and Zn atoms in parallel rows, for which the calculated vibrational CO_L frequency for CO at the saturation coverage was 2059 cm^{-1} and the adsorption energy 0.48 eV. The rearrangement of the atomic components on the surface from row to zigzag was calculated to affect structural and adsorptive properties while keeping essentially unchanged the electronic structure, reflecting the intermetallic character of PdZn on Pd(111).

Establishing the equivalent, the true origin of these bands on powder catalysts is not trivial. Owing to the complexity of the PdZn system, changes in composition and distribution of the nano-sized alloy with temperature, gas phase composition, exposure time, among others, could readily occur. Our observed trends of higher wavenumber and adsorption energy for CO on L_{II} sites, as compared with L_{III}, resemble those of Weilach et al.'s work on CO linearly bound to zigzag versus parallel Pd surface structure [12]. Be that as it may, and taking into account said seminal work of Rupprechter's team, it is tempting to assign the band located at 2070 cm^{-1} on our zinc-containing supported Pd catalyst (L_{II}) to CO linearly chemisorbed to a surface zigzag array of PdZn(111) alloyed atoms, while the lower frequency signal at 2035 cm^{-1} (L_{III}) would correspond to domains in which the PdZn alloy exhibits the conventional (in parallel rows) arrangement.

The appearance of a third, new CO_L band at approximately 2100 cm^{-1} (hereby designated as L_I) was only observed on the zinc-containing catalysts. After pre-reduction at 623 K this band was present from the onset of the CO chemisorption on the Pd/ZnO catalyst, but for Pd/ZnO–CeO_2 its progress with exposure time and/or CO pressure was remarkable (Fig. 3). In the case of the flat PdZn/Pd(111) surfaces mentioned above, the zigzag model for Pd atoms was theoretically sustained as a surface reconstruction induced and stabilized by the presence of CO in the gas phase. Yet, since CO(g) has a strong effect on pure-Pd supported-crystallite reconstruction [29], probably another

kind of surface rearrangement or dislocation can be thought of to explain the appearance and growth of the L_I band.

The chemisorbed CO IR signals reported by some of us using Pd/SiO_2 [29] are entirely similar to the ones that were found here for Pd/CeO_2. That is, in materials where no Pd bimetallic particles are formed, the L_I band is not observed. The CO adsorbate might operate, then, as a tell-tale detector of "isolated" Pd atoms in a Zn matrix.

This L_I band located at about 2100 cm^{-1} indicates a stronger C–O bond, most likely due to less electron retrodonation to the $2\pi^*$ molecular orbital of CO. An image consistent with this argumentative line is the presence of Pd atoms embedded into a zinc matrix, with less available *d* electrons than the metal atoms located on corners or edges of pure Pd crystallites. Another option, put forward by Gelin et al. [31], would be that of a shared CO_L and CO_B chemisorption, which we consider is a less appropriate alternative.

The congruence of our experimental results with former work in regard to Pd supported onto materials containing ZnO is straightforward, and truly indicates that a Pd–Zn surface alloy was formed on the ZnO–CeO_2 *nanocomposite* as well. Nevertheless, longer exposure time and/or higher CO pressure led to further morphological changes of the metal (nano)particles, as revealed by the onset and/or growth of CO_B bands. In other words, our results suggest that in presence of CO in the gas phase surface segregation of Pd and/or surface Pd ensemble formation already occurs at room temperature on these bimetallic PdZn supported-nanocrystallites.

The impact of using a lower pre-reduction temperature (T_{redn} = 423 K) on CO chemisorption at 10 and 50 Torr can be appreciated in Fig. 4. On Pd/CeO_2, the signals related to CO_L were not substantially modified by either CO pressure or exposure time, but noticeable surface reconstruction of Pd was observed with both, exposure time and superimposed pressure of the adsorbate, as indicated by the appearance and growth of the CO_H band, which is entirely similar to the reconstruction previously reported on Pd/SiO_2 catalysts [29]. For Pd/ZnO, in particular, the CO_B signals were stronger than those related to linearly coordinated CO. Our XPS data indicated that after H_2 reduction at this low temperature substantial amount of non-alloyed Pd crystallites still remained on Pd/ZnO and Pd/ZnO–CeO_2 but, also, that the percentage of PdZn domains was higher in the catalyst synthesized with the *nanocomposite* support (see Table 2), which is congruent with the overall IR features shown in Fig. 4.

The progressive alloying of Pd with reduction temperature can be fully appreciated in Fig. 5, where the initial CO chemisorption spectra, taken at 0 min (10 Torr CO) after pre-reducing the catalysts at progressively higher temperature, are compared. As a general trend, it can be observed that the total amount (integrated absorbance area) of the CO chemisorbed onto the ZnO-containing catalysts decreased

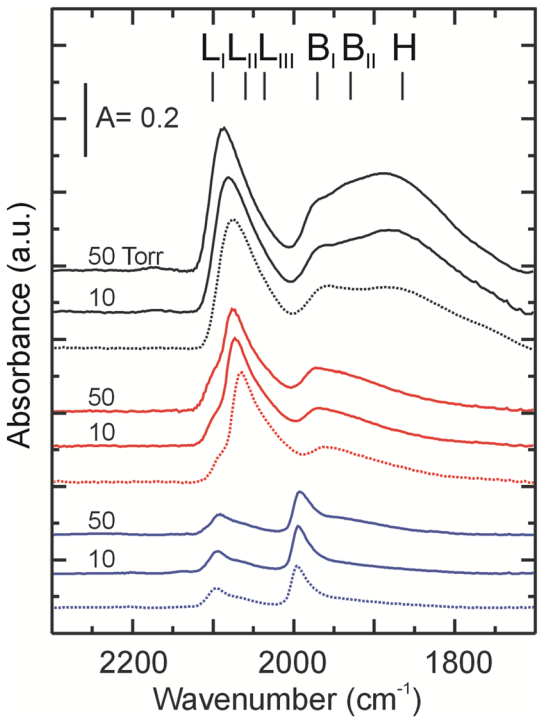

Fig. 4 Static chemisorption of CO at RT on the Pd/CeO_2 (black), Pd/ZnO–CeO_2 (red), and Pd/ZnO (blue) catalysts pre-reduced in pure H_2 at 423 K. Dashed and full lines correspond to 0 and 10 min exposure time, respectively

steadily the higher the reduction temperature was, but it increased again after reducing at 623 K. Moreover, the L_I band (i.e., CO chemisorbed on "isolated" Pd sites) became more distinct after the highest reduction temperature.

Next, the combined, integrated absorbance of the linear (CO_L), dicoordinated (CO_B) and tricoordinated (CO_H) CO chemisorbed on the catalysts upon exposing them to 10 Torr CO (0 and 10 min) after H_2 pre-reduction at 423, 473, 523, 573 and 623 K (protocol A) or, else, after pre-reduction at 623 K followed by CO_2 pre-adsorption and evacuation at RT (protocol B) were calculated in detail (see Table S1 in Online Resource 1). From now on, for simplicity, $CO_{\Sigma L}$ stands for $CO_{LI} + CO_{LII} + CO_{LIII}$ and, likewise, $CO_{\Sigma(B+H)}$ represents $CO_{BI} + CO_{BII} + CO_H$. These $CO_{\Sigma L}$ and $CO_{\Sigma(B+H)}$ values, as a function of the pre-reduction temperature, are shown in Fig. 6 for each catalyst. It is apparent that the integrated absorbances on Pd/CeO_2 were noticeably higher than those for the other materials. Also, it is worth to point out that on this catalyst the B (and H) bands were more intense than the L bands for the entire range of pre-reduction temperatures, which is more clearly shown in Fig. 7, which depicts the corresponding $CO_{\Sigma L}/CO_{\Sigma(B+H)}$ ratios.

On the Pd/ZnO–CeO_2 catalyst, besides the observed preponderance of the L_I band mentioned above, it can be appreciated in Figs. 6 and 7 that the differences in absorbance

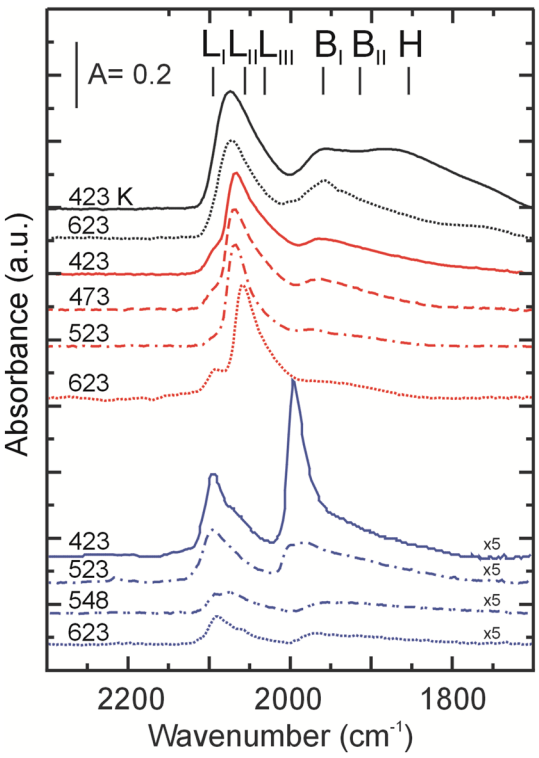

Fig. 5 Static chemisorption of CO (10 Torr) at RT on the Pd/CeO_2 (black), Pd/ZnO–CeO_2 (red), and Pd/ZnO (blue) catalysts pre-reduced in pure H_2 at different, increasing temperatures. Initial spectra (t = 0 min)

intensity between the $CO_{\Sigma L}$ and $CO_{\Sigma(B+H)}$ bands became larger for $T_{redn} > 500$ K, the former ones always prevailing over the latter. This last fact is straightly observed in Fig. 7, which shows that the $CO_{\Sigma L}/CO_{\Sigma(B+H)}$ ratio recorded upon the initial exposure to CO (t = 0 min) increased substantially for higher T_{redn} on the ZnO–CeO_2 *nanocomposite* supported-Pd. Similar results were found recently by Gallagher et al. on Pd–Zn/Al_2O_3 powder catalysts, using DRIFT [14].

The formation of intermetallic compounds and/or alloys during H_2 reduction has been reported for Pd, Pt and Rh supported on CeO_2 above 773 K [32, 33]. Much lower T_{redn} was used here, which grants disregarding any Pd–Ce bimetallic formation. Also, although it is widely known that strong metal-support interaction (SMSI) effects can occur upon Pd/CeO_2 reduction, leading to Pd crystallites partially occluded by CeO_x patches (and hence to smaller CO chemisorption values), Kepinski and Wolcyrz [34] reported SMSI effects in Pd/CeO_2 only after reduction above 973 K. Therefore, no SMSI effect on Pd/CeO_2 under our experimental conditions was expected. The CO_H band was the highest growing feature with exposure time and/or CO superimposed pressure on this catalyst for lower T_{redn} (Figs. 2, 3). However, the surface-exposed metal fraction, SEF, of the Pd particles was not modified with the pre-reduction temperature (about 25% either at $T_{redn} = 423$ or 623 K, Table 1), which suggests that crystallites annealing—together with strong bonding between the supported metal and the ceria- are concurrent explanations of this phenomenological pattern.

As pointed out above, in the case of the Pd/ZnO catalyst it was observed that the $CO_{\Sigma L}/CO_{\Sigma(B+H)}$ ratio was higher the higher the T_{redn} was (both at 0 and 10 min). Interestingly, on Pd/ZnO–CeO_2 the initial $CO_{\Sigma L}/CO_{\Sigma(B+H)}$ ratio showed an inflection point ($T_{redn} \sim 500$ K) and then increased, considerably, due to the almost disappearance of the CO_{B+H} bands. This indicates that above said reduction temperature the Pd atoms were already forming PdZn bimetallic surface domains, with Pd interatomic distances that precluded bridged and/or hollow CO adsorption. With exposure time to the adsorbate (10 min), these surface domains became restructured, as suggested by the decreased $CO_{\Sigma L}/CO_{\Sigma(B+H)}$ ratio (Fig. 7b, open symbols).

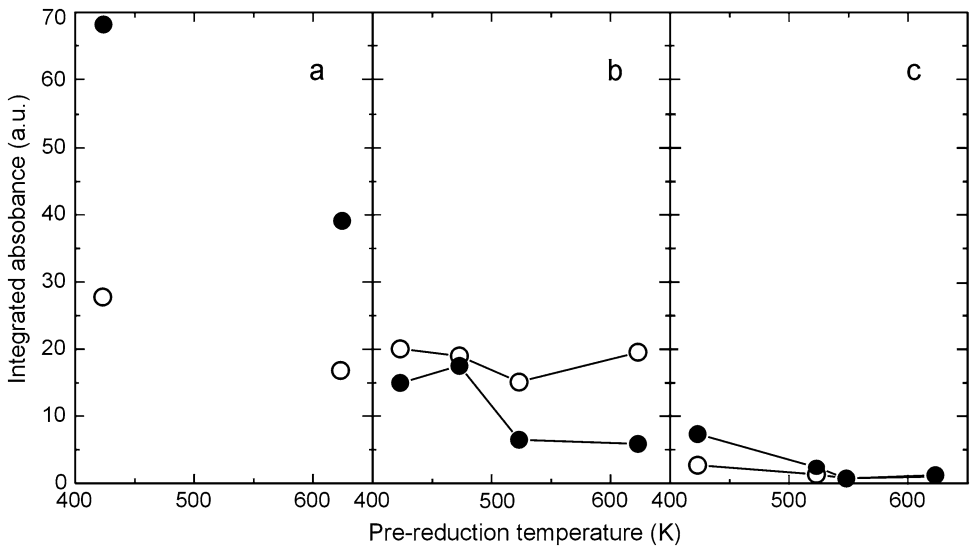

Fig. 6 Integrated absorbance of linearly [$CO_{\Sigma L}$, open symbols] and di + tricoordinated [$CO_{\Sigma(B+H)}$, full symbols] chemisorbed CO versus pre-reduction temperature, T_{redn}, on: **a** Pd/CeO_2, **b** Pd/ZnO–CeO_2, and **c** Pd/ZnO (RT; 10 Torr CO; 0 min)

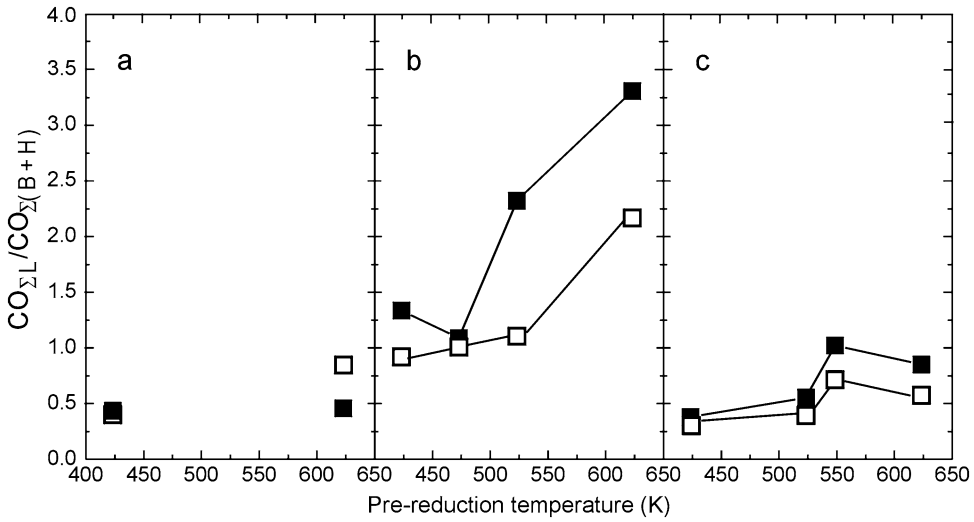

Fig. 7 Evolution with time of the ratio of the integrated absorbance of linearly and di + tricoordinated chemisorbed CO: $CO_{\Sigma L}/CO_{\Sigma(B+H)}$, after different pre-reduction temperatures, on: **a** Pd/CeO_2, **b** $Pd/ZnO\text{-}CeO_2$, and **c** Pd/ZnO (RT; 10 Torr CO; full symbols: 0 min; open symbols: 10 min)

A closer look to CO chemisorption on Pd/ZnO (Fig. 7) reveals that the inflection related to the Pd-Pd distance increase after H_2 pre-reduction also took place on this catalyst, but at higher T_{redn} than supported-Pd on the $ZnO–CeO_2$ *nanocomposite*. On Pd/ZnO resp. $Pd/ZnO–CeO_2$, the formation of the PdZn alloy might have been kinetically limited, owing to the different supports textures (Table 1).

The phase diagram of the Pd–Zn system indicates that the tetragonal (β_1) alloy, PdZn (1:1 atom/atom) is the most stable one, together with the cubic phases, enriched in either Pd (β'') or Zn (β) [35]. The β_1-PdZn alloy has been found particularly active for the MSR reaction [11, 15, 36], but these alloys are known to interconvert. The bulk solid phase melts at approx. 923 K, but nanoparticles 'melting point' can lie well below the Tamman´s temperature. Nonetheless, albeit the presence of no particular PdZn phase is claimed here (the low wt% content of Pd would not allow XRD detection), the dynamic structure of these surface alloys, as revealed by the L_I, L_{II} and L_{III} bands of chemisorbed CO is evident.

In this regard, Fig. 7 shows that for each Zn-containing catalyst the $CO_{\Sigma L}/CO_{\Sigma(B+H)}$ ratio decreased with CO (10 Torr) exposure time for every pre-reduction temperature, owing to the surface restructuring of Pd. This restructuring process, which was more evident after higher T_{redn}, reveals the flexible character of the Pd(Zn) surface nanoparticles.

To inquire further about the (possible) degree of reversibility of the restructuring phenomenon, a second CO chemisorption at RT was made on the catalysts right after the temperature-programmed desorption of the adsorbate up to 623 K (Fig. 8). For the Zn-containing materials, the important presence of bridge-bonded CO (CO_B bands) from the onset of the CO chemisorption, as well as its increasing growth with exposure time and/or CO pressure became apparent. Type L_I chemisorbed CO to PdZn surface domains were also observed at 0 min. The intensity of this band also

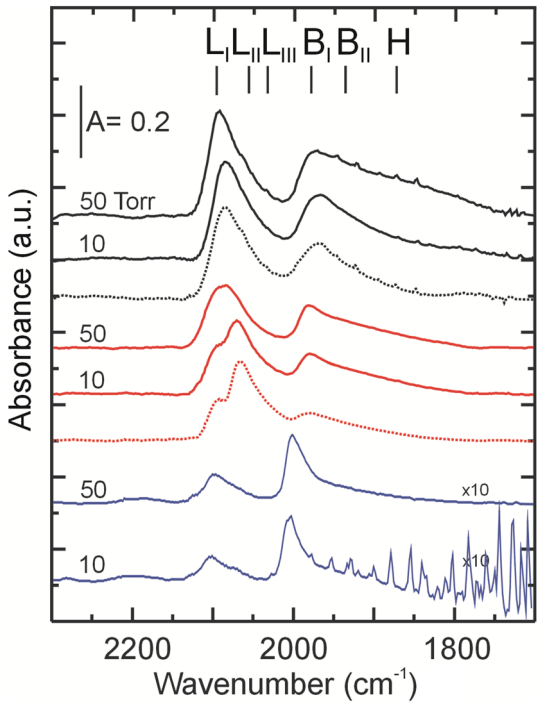

Fig. 8 Second static chemisorption of CO at RT on the Pd/CeO_2 (black), $Pd/ZnO–CeO_2$ (red), and Pd/ZnO (blue) catalysts pre-reduced at 623 K, after TPD (protocol A, see text). Dashed and full lines correspond to 0 and 10 min exposure time, respectively

grew with exposure time, but the total $CO_{\Sigma L}/CO_{\Sigma(B+H)}$ ratio (not shown) decreased after 10 min exposure.

So, the combined presence of the CO_{LI} and CO_B bands from the outset of the second chemisorption suggest that, even though the supported Pd had formed bimetallic PdZn particles upon H_2 pre-reduction of the catalysts at 623 K, these particles underwent (surface) restructuring during the first exposure to CO and subsequent TPD step, prior to the

second CO chemisorption, with (partial) segregation to surface Pd patches.

The impact of pre-exposing 'fresh samples' of the catalysts pre-reduced at 623 K to CO_2 (100 Torr; 10 min; RT) prior to the chemisorption of CO at room temperature (protocol B, step iii) can be appreciated in Fig. 9. On Pd/CeO_2 the IR spectra resembled the ones obtained upon exposing the catalyst to CO right after H_2 pre-reduction at 423 K (Fig. 4). However, a higher portion of CO_H is observed after CO_2 exposure, which might be attributed to the (partial) Pd surface reconstruction of the supported metal crystallite on a (now) carbonated ceria. On the zinc-containing supported Pd catalysts, on the other hand, the $CO_{\Sigma L}/CO_{\Sigma(B+H)}$ ratios measured at 0 min (10 Torr) were smaller than the ones measured on the corresponding fresh samples of the materials, i.e., exposed to CO right after H_2 pre-reduction at 423 K (for details see Table S1 at Online resource 1). Fast metal crystallites restructuring with exposure time, with distinct evidence of segregated Pd surface domains (notably the CO_B band), was also noted (Fig. 9). These combined observations suggest that the pre-exposure of the catalysts to CO_2 prior to CO chemisorption (even at this low temperature) modified substantially the stability of the PdZn (nano)alloys formed in the H_2 reduction step at 623 K and, also, the restructuring capability of the (nano)crystallites on these materials. We believe that this might have been most likely caused by the scavenging of Zn atoms, converted afterward into zinc (hydroxy)carbonates, which are readily produced on these supports upon CO_2 chemisorption at RT (see Fig. S1 at Online resource 1).

That is, exposure to CO_2 could be able to (partially) reoxidize Zn in the surface of the PdZn nanoalloy, leading to the formation of zinc (bi)carbonates, which can partially cover the surface of the bimetallic PdZn crystallites and/or "isolate" palladium atoms (responsible of the observed increase of the CO_{LI} band -in Pd/ZnO–CeO_2 catalyst-, previously assigned to that kind of Pd site).

3.3 Dynamic Isobaric Adsorption of CO (TPA-CO)

The evolution with temperature of chemisorbed CO on the Pd/CeO_2 and Pd/ZnO–CeO_2 catalysts under a steady stream of CO (1%)/He is shown in Fig. 10. The 'initial' spectra shown in the figure correspond to CO chemisorption after H_2 pre-reduction at 623 K followed by evacuation and exposure (30 min) to the flowing gas mixture at RT. The Pd/ZnO catalyst could not be studied by this technique because, owing to the low surface area of the support, the signal-to-noise ratio of the spectra was too low.

At room temperature, the band of CO_H—centered at about 1850 cm^{-1}—was predominant on Pd/CeO_2 and more intense than during the static CO chemisorption experiments, thus showing that intense restructuring of the metal crystallites had already taken place after the 30 min exposure to the flowing gas mixture at RT [29]. With heating, all

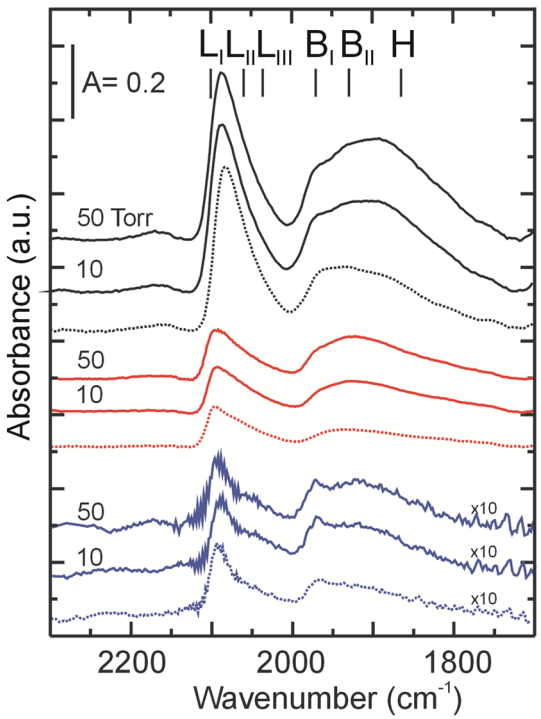

Fig. 9 Static chemisorption of CO at RT on the Pd/CeO_2 (black), Pd/ZnO–CeO_2 (red), and Pd/ZnO (blue) catalysts prereduced at 623 K, with further pre-exposure to CO_2 (RT, 100 Torr, 10 min) and evacuation. Dashed and full lines correspond to 0 and 10 min exposure time, respectively

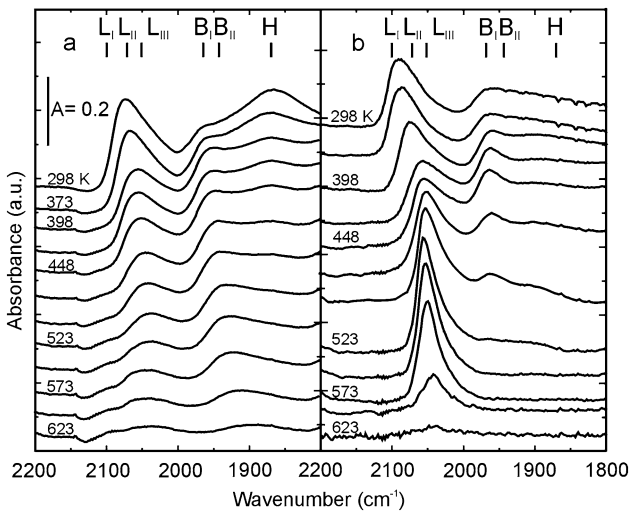

Fig. 10 Dynamic, temperature-programmed adsorption of CO (TPA-CO) on the Pd/CeO_2 (**a**), and Pd/ZnO-CeO_2 (**b**) catalysts. The first spectrum shown was taken after 30 min exposure to CO (1%)/He (50 cm^3/min)

the bands of adsorbed CO decreased in intensity, showing the classical red shift related to less dipole–dipole coupling at progressively smaller surface coverage with the chemisorbed adsorbate.

The FTIR spectra of the catalysts prepared with the composite support, Pd/ZnO–CeO_2, were completely dissimilar to the former ones. A sizable amount of linearly bonded CO was still present even above 550 K while the signals related to di or tricoordinated CO were no longer discernible. An attempt was made to evaluate (at least semi-quantitatively) the significance of these profound differences, and to assess them, employing the following assumptions: (a) the integrated absorbance of the IR bands is proportional to the amount of chemisorbed CO; (b) the values of the absorptivity coefficients are temperature-independent; and (c) chemisorption equilibrium holds at each temperature. The foundation for these assumptions was fully discussed in a previous work by some of us [37].

Figure 11 and S2 (see Online Resource 1) show the evolution with temperature of the integrated absorbance and the relative coverage (θ), respectively, of the linear ($CO_{\Sigma L}$) and di + tricoordinated ($CO_{\Sigma B+H}$) carbon monoxide onto both pre-reduced catalysts. The relative coverage was defined as the ratio between the integrated absorbance of the different types of chemisorbed CO species, at each temperature, versus their respective absorbance at 298 K after the 30 min exposure to the flowing CO (1%)/He gas mixture.

By observing the evolution of the integrated absorbance (or relative coverage) of the $CO_{\Sigma L}$ and $CO_{\Sigma B+H}$ bands on Pd/CeO_2 in Fig. 11 (or Fig. S2), it is apparent that the former decayed first, disappearing under 550 K, while some $CO_{\Sigma B+H}$ still remained on the surface even at 600 K.

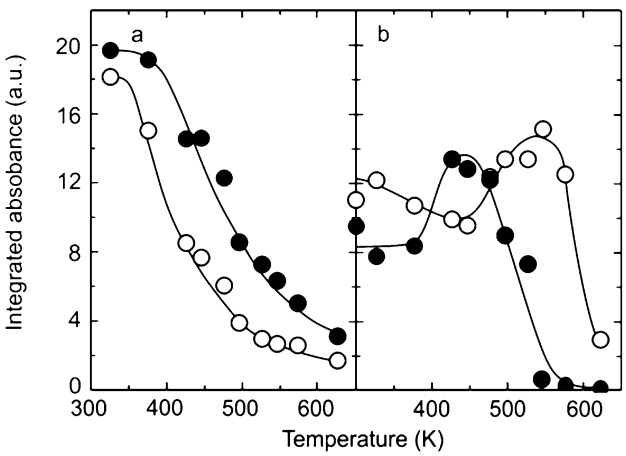

Fig. 11 Evolution with the temperature of the integrated absorbance of $CO_{\Sigma L}$ (open symbols) and $CO_{\Sigma(B+H)}$ (full symbols) on the Pd/CeO_2 (**a**) and Pd/ZnO–CeO_2 (**b**) catalysts under the flowing CO (1%)/He adsorption mixture

On this catalyst, like on Pd/SiO_2 [37], the linearly bonded species were more labile than the multicoordinated CO. Conversely, the Pd/ZnO–CeO_2 catalyst gave an entirely different TPA-CO pattern. Linearly bonded chemisorbed CO was more persistent (and abundant) at high temperature instead. Moreover, some apparent interconversion between the linear and multi-coordinated CO could also be appreciated with the progressive heating, thus showing that the dynamic nature of the PdZn surface alloys upon exposure to CO is kinetically controlled at low temperature. That is, despite the segregation of Pd surface domains able to adsorb CO as CO_B and CO_H species after 30 min exposure at RT in the flowing CO(1%)/He mixture (which were practically absent at 0 min of exposure time in the static adsorption experiments, Fig. 3, due to surface restructuring [29]), said segregation progressed with further heating under the superimposed CO pressure. Ultimately, though PdZn surface re-alloying at the expense of the Pd surface domains ensued. At 500 K, in fact, chemisorbed $CO_{\Sigma L}$ was almost as abundant as at room temperature on the Pd/ZnO–CeO_2 catalyst, and was the only species present over 550 K.

Scheme 1 shows the suggested surface changes for a supported bimetallic PdZn crystallite on ZnO–CeO_2, after exposure to CO at RT during 10 min and under the TPA-CO experiment.

A possible driving force for Pd domains migrating back into the PdZn surface alloy -or Zn coming back to the surface- would be to assume an endothermic process for the PdZn surface re-alloying under gaseous CO. To the best of our knowledge, thermodynamic (experimental) data of PdZn surface alloys are unknown. However, it is known that the β_1-PdZn (bulk) alloy formation is exothermal but, *and* also, that dramatic changes of the activity of Zn occur across the homogeneous range (by two orders of magnitude change within two atomic percent at the stoichiometric composition) on these alloys [38]. So, further research is needed to clarify this point, which is beyond the aim of this work.

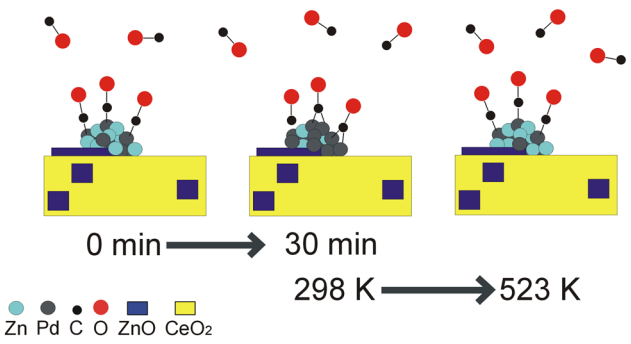

Scheme 1 Suggested surface reconstruction of the bimetallic PdZn crystallite supported on a ZnO–CeO_2 *nanocomposite*

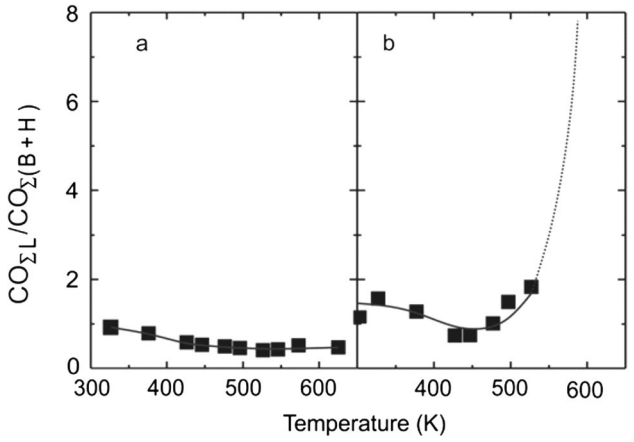

Fig. 12 Evolution with the temperature of the ratio of the integrated absorbance of linear and di + tricoordinated chemisorbed CO: $CO_{\Sigma L}$ / $CO_{\Sigma(B+H)}$, on the Pd/CeO_2 (**a**) and Pd/ZnO–CeO_2 (**b**) catalysts under the flowing CO (1%)/He adsorption mixture

This strikingly distinct interaction between the 'inert' CeO_2 and the 'reactive' ZnO–CeO_2 *composite* oxide with the supported palladium can be fully appreciated in Fig. 12, which shows the evolution of the $CO_{\Sigma L}/CO_{\Sigma(B+H)}$ ratio during the TPA-CO study. Such ratio was close to one on Pd/CeO_2, and decreased with heating temperature, whereas dramatically increased instead, well beyond unity, for the catalyst prepared with the Zn-containing *composite* support. This growth of the $CO_{\Sigma L}/CO_{\Sigma(B+H)}$ ratio above 500 K, attributed to the stabilization of the linearly bonded, chemisorbed CO onto bimetallic PdZn particles, evidences that CO is a useful indicator of the presence of surface PdZn alloying, which is in agreement with the results of Föttinger [18] and Collins et al. [5] for intermetallic Pd–Zn/ZnO and Pd–Ga/Ga_2O_3.

In contrast to what it was found on Pd/CeO_2 and Pd/SiO_2, the palladium catalyst prepared using the Zn-containing *composite* support was fairly selective for the steam reforming of methanol, with selectivity to carbon dioxide above 65%, whereas the former were completely unselective [16]. Under MSR reaction conditions, then, Pd–Zn alloying efficiently prevented methanol decomposition (MD), which is prevalent whenever pure-Pd surface domains are present on these catalysts.

4 Conclusions

In the present study we have investigated the surface composition by X-ray photoelectron spectroscopy and the CO adsorption by infrared spectroscopy on a set of 2 wt% Pd catalysts supported on CeO_2, ZnO and a ZnO–CeO_2 *nanocomposite* to unveil the surface nature of bimetallic PdZn crystallites, after H_2 reduction in a wide range of temperature (423–623 K). XPS data showed a BE shifting of the Pd $3d_{5/2}$ signal, which suggested that more than 90% of Pd was zinc-alloyed at the highest reduction temperature for the Zn-based catalysts, as confirmed by the presence of metallic zinc.

Static IR transmission experiments under 10 Torr CO and 298 K showed the progressive formation of a supported-PdZn alloy after increased reduction temperature, revealed by the suppression of the CO_B and CO_H bands and the dominant prevalence of the CO_L signal at initial CO exposure time. The CO_L peak was ascribed to the result of three convoluted bands (L_I, L_{II}, and L_{III}), attributed to different degrees of surface Pd coordination, mainly due to the true formation of a surface PdZn alloy in the bimetallic particles. However, higher exposure time and/or higher CO pressure (50 Torr) degraded the surface alloy—even at 298 K—as suggested by the development of the CO_B and CO_H bands which, in other words, indicated the generation (segregation) of Pd surface ensembles similar to the existing on pure Pd crystallites. Carbonate(s) formation on the reduced catalyst supports after the pre-adsorption of CO_2—also at 298 K—did not significantly modify the nature of CO chemisorption on the (bi)metallic crystallites.

The temperature-programmed, dynamic isobaric adsorption of CO (TPA-CO), under flowing CO (1%)/He on the catalysts pre-reduced at 623 K (i.e., for similar conditions as those found in the MSR process) showed the conventional behavior for the desorption of CO on Pd/CeO_2, that is: both $CO_{\Sigma L}$ and $CO_{\Sigma(B+H)}$ started to desorb immediately after heating the sample. A contrasting picture was observed on the Pd/ZnO–CeO_2 catalyst: the total amount of adsorbed CO decreased only at $T > 473$ K, and the relative coverage of $CO_{\Sigma(B+H)}$ and $CO_{\Sigma L}$ showed maximum values at 423 and 523 K, respectively, with a fractional coverage of linear CO species, $\theta(CO_{\Sigma L})$, at 573 K close to the one at 298 K. In other words, these observations suggested a strong reconstruction of the bimetallic PdZn crystallite surface, leading to the re-generation of the PdZn domains (where the Pd–Pd distances became increased), proving the flexible nature of the alloyed metallic nanoparticles.

Acknowledgements The authors acknowledge financial support for this work from the ANPCyT of Argentina (PICT-2012-1280, PICT-2015-3651 and PME-2006-311) and Universidad Nacional del Litoral (CAID 2011 PI 50120110100311). C.B. thanks CONICET for the fellowship received to do this work.

Compliance with Ethical Standards

Conflict of interest The authors declare that there is no conflict of interest regarding the publication of this article.

References

1. Rebelli J, Detwiler M, Ma S, Williams CT, Monnier JR (2010) J Catal 270:224
2. Rebelli J, Rodríguez AA, Ma S, Williams CT, Monnier JR (2011) Catal Today 160:170
3. Rades T, Borovkov VY, Kazansky VB, Polisset-Thfoin M, Fraissard J (1996) J Am Chem Soc 100:16238
4. Kovnir K, Ambrüster M, Teschner D, Venkov TV, Szentmiklósi I, Jentoft FC, Knop-Gercke A, Grin Y, Schögl R (2009) Surf Sci 603:1784
5. Collins SE, Delgado JJ, Mira C, Calvino JJ, Bernal S, Chiavassa DL, Baltanás MA, Bonivardi AL (2012) J Catal 292:90
6. Föttinger K, Rupprechter G (2014) Acc Chem Res 47:3071
7. Lebarbier V, Dagle R, Conant T, Vohs JM, Datye AK, Wang Y (2008) Catal Lett 122:223
8. Eswaramoorthi I, Dalai AK (2009) Int J Hydrog Energy 34:2580
9. Conant T, Karim AM, Lebarbier V, Wang Y, Girgsdies F, Schlögl R, Datye A (2008) J Catal 257:64
10. Pfeifer P, Schubert K, Liauw MA, Emig G (2004) Appl Catal A 270:165
11. Föttinger K, van Bokhoven JA, Nachtegaal M, Rupprechter G (2011) J Phys Chem Lett 2:428
12. Weilach C, Kozlov SM, Holzapfel HH, Föttinger K, Neyman KM, Rupprechter G (2012) J Phys Chem C 116:18768
13. Stadlmayr W, Rameyan C, Weilach C, Lorenz H, Hävecker M, Blume R, Rocha T, Teschner D, Knop-Gericke A, Zemlyanov D, Penner S, Schlögl R, Rupprechter G, Klötzer B, Memmel N (2013) J Phys Chem C 114:10850
14. Gallagher JR, Childers DJ, Zhao H, Winans RE, Meyer RJ, Miller JT (2015) Phys Chem Chem Phys 17:28144
15. Rameshan C, Weilach C, Stadlmayr W, Penner S, Lorenz H, Hävecker M, Blume R, Rocha T, Teschner D, Knop-Gericke A, Schlögl R, Zemlyanov D, Memmel N, Rupprechter G, Klötzer B (2010) J Catal 276:101
16. Barrios CE, Bosco MV, Baltanás MA, Bonivardi AL (2015) Appl Catal B 179:262
17. Vecchietti MJ, Bonivardi AL, Xu W, Stacchiola D, Delgado JJ, Calatayud M, Collins SE (2014) ACS Catal 4:2088
18. Föttinger K (2013) Catal Today 208:106
19. Penner S, Jenewein B, Gabasch H, Klötzer B, Wang D, Knop-Gericke A, Schlögl R, Hayek K (2006) J Catal 241:14
20. Tao FF, Ralston WT, Liu H, Somorjai GA (2018) J Phys Chem B 122:425
21. Barrios CE, Baltanás MA, Bolmaro R, Bonivardi AL (2014) Powder Technol 267:180
22. Wagner CD, Riggs WN, Davis LE, Moulder JF, Muilenberg GE (1979) Handbook of X-ray photoelectron spectroscopy. Perkin-Elmer Corp., Eden Prairie
23. Iwasa N, Ogawa N, Masuda S, Takezawa N (1998) Bull Chem Soc Jpn 71:1451
24. Iwasa N, Yoshikawa M, Nomura W, Arai M (2006) Appl Catal A 292:215
25. Schön G (1973) J Electron Spectrosc Relat Phenom 2:75
26. Antonides E, Janse EC, Sawatzky GA (1977) Phys Rev B 15:1669
27. Badri A, Binet C, Lavalley JC (1996) J Phys Chem 100:8363
28. Lear T, Marshall R, López-Sánchez JA, Jackson SD, Klapötke TM, Bäumer M, Rupprechter G, Freund H-J, Lennon D (2005) J Chem Phys 123:174706 1
29. Cabilla GC, Bonivardi AL, Baltanás MA (1998) Catal Lett 55:147
30. Blyholder G (1964) J Chem Phys 68:2772
31. Gelin P, Siedle AR, Yates JT Jr (1984) J Phys Chem 88:2978
32. Bernal S, Calvino JJ, Cauqui MA, Gatica JM, Larese C, Pérez-Omil JA, Pintado JM (1999) Catal Today 50:175
33. Bernal S, Calvino JJ, Cifredo GA, Laachir A, Perrichon V, Herrmann JM (1994) Langmuir 10:717
34. Kepinski L, Wolcyrz M (1997) Appl Catal A 150:197
35. Peterson EJ, Halevi B, Kiefer B, Spilde MN, Datye AK, Peterson J, Daemen L, Llobet A, Nakotte H (2011) J Alloys Compd 509:1463
36. Halevi B, Peterson EJ, de La Riva A, Jeroro E, Lebarbier VM, Wang Y, Vohs JM, Kiefer B, Kunkes E, Havecker M, Behrens M, Schögl R, Datye AK (2010) J Phys Chem C 114:17181
37. Collins SE, Baltanás MA, Bonivardi AL (2008) J Mol Catal A 281:73
38. Kou S, Chang YA (1975) Acta Metall 23:1185

Affiliations

Celina E. Barrios[1] · Miguel A. Baltanás[1] · Marta V. Bosco[1] · Adrian L. Bonivardi[1,2]

✉ Adrian L. Bonivardi
abonivar@santafe-conicet.gov.ar

[1] Instituto de Desarrollo Tecnológico para la Industria Química, Universidad Nacional del Litoral and CONICET, Güemes 3450, 3000 Santa Fe, Argentina

[2] Facultad de Ingeniería Química, Universidad Nacional del Litoral, Santiago del Estero 2829, 3000 Santa Fe, Argentina